AIAA JOURNAL
Vol. 39, No. 12, December 2001

Unsteady Dynamic Variables Method for Heterogeneous Solid Propellant Burning

Sergey T. Surzhikov* and Herman Krier†
University of Illinois at Urbana–Champaign, Urbana, Illinois 61801

An extension of the vortex–stream function method is developed for solving two-dimensional gas flows at low Mach numbers ($M < 0.1$) near localized heat release regions. The method allows simulation of the locally heated unsteady gas flows for a wide range of density changes in the computational domain. Based on the developed method, a two-dimensional gasdynamic model for a multicomponent burning process is presented. The coupled, two-dimensional Navier–Stokes equations, with the conservation of energy and species and the conservation of mass, comprise the model. Temperature dependencies for the gas thermophysical properties are taken into account in the range of 500–3000 K. Solutions using the vortex–stream function method are presented that describe the microflame structures for the combustion of a prescribed array of ammonium perchlorate oxidizer and a hydroxyl-terminated polybutadiene binder, the fuel.

I. Introduction

THE main objective of the paper is to establish a new method for the numerical simulation of unsteady flows of viscous compressible gas at essentially subsonic speeds but with large changes density. Although the solution of the Navier–Stokes equations with chemical reactions is routinely done,[1,2] in the unsteady problem considered here, the complications of the coupled heat transfer to the solids and surface pyrolysis leads to the need to resolve wide ranges of timescales for both the acoustic and gasdynamic processes.

The general idea of our method is to solve the gasdynamic equations using dynamic variables (vortex–stream function), where pressure is excluded from the motion equations. It has been established for some steady-state problems that methods using dynamic variables may be more efficient in some cases than methods using primitive variables (velocity–pressure variables), especially for the two-dimensional problems.[1–3] However, as is well known, dynamic variables cannot be employed when unsteady compressible gas movement is considered.

The proposed method, unsteady dynamic variables (UDV), allows one to stay within the framework of an approach that implements vortex–stream function variables and to preserve its higher efficiency. It will be shown that this can be achieved by the introduction of a new function, which required an additional transfer equation to be solved.

II. Mathematical Formulation of the Problem and the UDV Method

The conservation relation for these viscous, conducting, and chemically reacting flows may be considered as three groups for the gas phase, that is, the Navier–Stokes conservation of momenta (with continuity), the energy conservation, and the species conservation.

Because the main objective of this study is to develop the UDV method for solving a system of gasdynamics equations, we will start with a description of the method, and the full system for describing chemically reacting, viscous, and heat conductive gas with the new variables will be formulated later.

We will assume here that the density of the gas and its time derivative are known coordinate functions. Our task is to calculate the velocity field in free space surrounding the area of a local gas heating.

We will use a system of Navier–Stokes and continuity equations in a two-dimensional Cartesian's coordinates system (see Fig. 1). These are

$$\frac{\partial \rho}{\partial t} + \operatorname{div}(\rho \boldsymbol{V}) = 0 \tag{1}$$

$$\frac{\partial \rho u}{\partial t} + \operatorname{div}(\rho u \boldsymbol{V}) = -\frac{\partial p}{\partial x} + S_u + \rho a \tag{2}$$

$$\frac{\partial \rho v}{\partial t} + \operatorname{div}(\rho v \boldsymbol{V}) = -\frac{\partial p}{\partial y} + S_v \tag{3}$$

where S_u and S_v are the components of the stress tensor divergence,

$$S_u = -\frac{2}{3}\frac{\partial}{\partial x}(\mu \operatorname{div} \boldsymbol{V}) + \frac{\partial}{\partial y}\left[\mu\left(\frac{\partial u}{\partial y} + \frac{\partial v}{\partial x}\right)\right] + 2\frac{\partial}{\partial x}\left(\mu \frac{\partial u}{\partial x}\right) \tag{4}$$

$$S_v = -\frac{2}{3}\frac{\partial}{\partial y}(\mu \operatorname{div} \boldsymbol{V}) + \frac{\partial}{\partial x}\left[\mu\left(\frac{\partial u}{\partial y} + \frac{\partial v}{\partial x}\right)\right] + 2\frac{\partial}{\partial y}\left(\mu \frac{\partial v}{\partial y}\right) \tag{5}$$

where x and y are the longitudinal and transversal coordinates; u and v are the projections of the flow speed $\boldsymbol{V}$ on the x and y axes; ρ, p, and μ are the density, pressure, and viscosity, respectively; and a is the projection of the gravitational acceleration on the x axis.

To obtain the equations to be numerically integrated, we will apply a procedure typical for the dynamic variables method. Equation (2) will be differentiated with respect to y, and Eq. (3) will be differentiated with respect to x, after which we will subtract the first equation from that result, to obtain an equation that does not contain the pressure. Thus,

$$\frac{\partial \omega}{\partial t} + \frac{\partial}{\partial x}\operatorname{div}(\rho v \boldsymbol{V}) - \frac{\partial}{\partial y}\operatorname{div}(\rho u \boldsymbol{V}) = \frac{\partial S_v}{\partial x} - \frac{\partial S_u}{\partial y} - a\frac{\partial \rho}{\partial y} \tag{6}$$

where a new (vorticity) variable is introduced:

$$\omega \equiv \frac{\partial \rho v}{\partial x} - \frac{\partial \rho u}{\partial y} \tag{7}$$

When the two divergent components are combined, Eq. (6) will be transformed as follows:

$$\frac{\partial \omega}{\partial t} + \operatorname{div}(\omega \boldsymbol{V}) + \frac{\partial}{\partial x}\left(\rho v \frac{\partial u}{\partial x} - \rho u \frac{\partial u}{\partial y}\right) + \frac{\partial}{\partial y}\left(\rho v \frac{\partial v}{\partial x} - \rho u \frac{\partial v}{\partial y}\right) = \frac{\partial S_v}{\partial x} - \frac{\partial S_u}{\partial y} - a\frac{\partial \rho}{\partial y} \tag{8}$$

Received 19 August 2000; revision received 6 June 2001; accepted for publication 11 June 2001.

*Visiting Research Professor; currently Head of the Computational Physical-Chemical and Radiative Gas Dynamics Laboratory, Institute for Problems in Mechanics, Russian Academy of Sciences, Prospect Vernadskogo 101, 117526, Moscow, Russia; surg@ipmnet.ru. Member AIAA.

†Professor, MC-244, Department of Mechanical/Industrial Engineering, 1206 West Green Street; h-krier@uiuc.edu. Fellow AIAA.

To obtain the second equation of the system to be identified, we will use the continuity equation. It can serve as the basis for introducing the stream function ψ, but only in the following two particular cases: 1) when the stream is incompressible, that is, div $\boldsymbol{V} = 0$, and 2) when a stationary solution of compressible gas movement is to be found, that is, div $\rho \boldsymbol{V} = 0$.

Identical satisfaction to one of the mentioned consequences of the continuity equation allows one to obtain the relations required for identification of the stream function. For instance,

$$\rho u = \frac{\partial \psi}{\partial y}, \qquad \rho v = -\frac{\partial \psi}{\partial x}$$

It is easy to see that the introduction of the stream function is not possible in the general case of unsteady compressible gas flows. To stay within the framework of the dynamic variables method, we will introduce a new scalar function $E \neq -1$ complying with the following equation:

$$\operatorname{div}(E\rho \boldsymbol{V}) = \frac{\partial \rho}{\partial t} \tag{9}$$

The form of Eq. (9), which specifies the E function, is dictated by the possibility of introducing a modified stream function Ψ, which satisfies the continuity equation,

$$\operatorname{div}[(1+E)\rho \boldsymbol{V}] = 0 \tag{10}$$

namely,

$$\frac{\partial \Psi}{\partial y} = (1+E)\rho u, \qquad \frac{\partial \Psi}{\partial x} = -(1+E)\rho v \tag{11}$$

Equations (11) serve to determine projections of the mass flow to the coordinate axes after the fields of functions ω and Ψ have been found. Note that Eqs. (11) can also be expressed as

$$\rho u = \frac{1}{(1+E)}\frac{\partial \Psi}{\partial y}, \qquad \rho v = -\frac{1}{(1+E)}\frac{\partial \Psi}{\partial x} \tag{12}$$

It is obvious that the lack of a condition that limits the modification of the function E causes difficulties in the computational procedure for the identification of the mass flow components, as $E \to -1$. Therefore, we will use the substitution

$$\varepsilon = \ell n(1+E) \tag{13}$$

Initially this substitution does not appear to change anything because it retains the computational peculiarity at $E \to -1$. However, when Eq. (9) is formulated in relation to the function ε, this allows one to make the modification range of function ε more specific. To obtain the target equation, we will use Eq. (9) recorded as follows:

$$E \operatorname{div} \rho \boldsymbol{V} + \rho \boldsymbol{V} \operatorname{grad} E = \frac{\partial \rho}{\partial t}$$

By substituting div $\rho \boldsymbol{V}$ by the time derivative of density, we will obtain

$$\rho \boldsymbol{V} \operatorname{grad}[\ell n(1+E)] = \frac{\partial \rho}{\partial t}$$

or, in a form more convenient for integration,

$$\rho u \frac{\partial \varepsilon}{\partial x} + \rho v \frac{\partial \varepsilon}{\partial r} = \frac{\partial \rho}{\partial t} \tag{14}$$

Taking into account the function ε determined in such a way, we will obtain the following relation between the mass flow vector components and the Ψ-function gradient components:

$$\frac{\partial \Psi}{\partial y} = \exp(\varepsilon)\rho u, \qquad \frac{\partial \Psi}{\partial x} = -\exp -(\varepsilon)\rho v \tag{15}$$

The last equation of the formulated system establishes relation between functions ω and Ψ. We will use the definition given in Eq. (7) for the function ω and insert relations (13) to obtain

$$\operatorname{div}[\exp(-\varepsilon \operatorname{grad} \Psi)] = -\omega \tag{16}$$

Thus, instead of the system of Eqs. (1–3) we now have Eq. (8) for determining the function ω, Eq. (16) for determining the Ψ function, and Eq. (14) for determining the new function ε. Relations (15) allow one to calculate the mass flow vector components. A sequence of solving these equations will be defined in Sec. IX.

We should also comment upon the introduced functions ω, ε, and Ψ.

First, the function ω is called the vortex function because this is an azimuth component of vector curl$(\rho \boldsymbol{V})$. This is a consequence of that the mentioned procedure to obtain Eq. (6) is a full analog of the application of the curl operator with Navier–Stokes equations recorded in the form of one equation in relation to vector function $\rho \boldsymbol{V}$. Note that dynamic variables method ψ–ω used previously to solve the problems of compressible and incompressible gasdynamics defined function ω only in a role related to the velocity components:

$$\omega = \frac{\partial v}{\partial x} - \frac{\partial u}{\partial r}$$

Second, the nonstationary stream function Ψ is an analog of the stream function ψ in terms of the definition, kind, and method of usage. At $\varepsilon \to 0$, which corresponds to an established stream, function Ψ automatically becomes ψ.

Third, the function ε (or E) may be considered as a measure of the unsteady character of the gas flow thermal condition. Conditions $\varepsilon \to 0$ or $E \to 0$ are met at steady state, which leads to an asymptotic transition to simple dynamic variables.

Last, note that by its definition the stream function has a distinct physical sense: The value $\Psi(y)$ enters the total flow rate of the gas through the layer with width y located perpendicular to the x axis [in our case the flow rate is adjusted by value $(1+E)$].

The clear physical sense of the function ε resulting from the definition allows one to formulate the boundary conditions. In particular, if the temperature does not change with time at a certain area boundary, then the condition $\varepsilon = 0$ can be used.

III. Formulation of the Full System of Equations

The UDV method will be used to investigate the microflames structure near the burning surface of heterogeneous solid propellants. The schematic of the problem is shown in Fig. 1. A detailed discussion of the physical problem statement is presented in Ref. 4. Here we present the full system of equations needed to solve the problem in the scope of a computing model, with attention focused on the numerical simulation aspects. This system of equations takes into account gasdynamic and mass transfer processes near the burning surface and also heat transfer processes. Two chemical kinetic models and a state equation are used for closing these equations.

When the unsteady dynamic variables are used, the system of equations describing the slow movement of viscous, heat

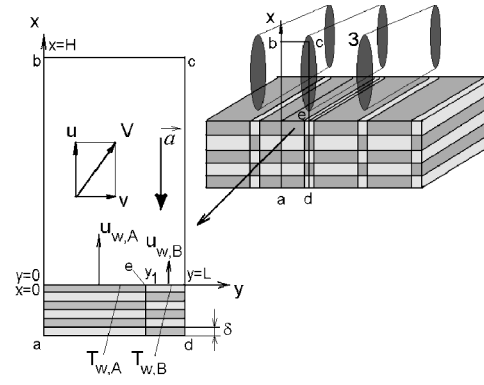

Fig. 1 Schematic of the domain to solve for the combustion above layers of AP/binder solid propellant.

conducting, and chemically reacting gas is represented by the following relations:

$$\frac{\partial\omega}{\partial t}+\operatorname{div}(\omega \boldsymbol{V})+\frac{\partial}{\partial x}\left(\rho v\frac{\partial u}{\partial x}-\rho u\frac{\partial u}{\partial y}\right)+\frac{\partial}{\partial y}\left(\rho v\frac{\partial v}{\partial x}-\rho u\frac{\partial v}{\partial y}\right)$$
$$=\frac{1}{Re}\left(\frac{\partial S_v}{\partial x}-\frac{\partial S_u}{\partial y}\right)-\frac{1}{Fr^2}\frac{\partial\rho}{\partial y} \tag{17}$$

$$\operatorname{div}[\exp(-\varepsilon)\operatorname{grad}\Psi]=-\omega \tag{18}$$

$$\rho u\frac{\partial\varepsilon}{\partial x}+\rho v\frac{\partial\varepsilon}{\partial r}=\frac{\partial\rho}{\partial t} \tag{19}$$

$$\frac{\partial\Psi}{\partial y}=\exp(\varepsilon)\rho u,\qquad \frac{\partial\Psi}{\partial x}=-\exp(\varepsilon)\rho v \tag{20}$$

$$\rho c_p\frac{\partial T}{\partial t}+\rho c_p V\operatorname{grad}T=\frac{1}{Pr\,Re}\operatorname{div}(\lambda\operatorname{grad}T)+\frac{1}{Re\,Sc}\sum_{k}^{N_c}$$
$$\times c_{p,k}\rho D_k(\operatorname{grad}Y_k\cdot\operatorname{grad}T)+\sum_{k}^{N_c}h_k\varpi_k\left(\frac{L}{\rho_0 c_{p,0}u_0}\right) \tag{21}$$

$$-\varpi_k\frac{L}{\rho_0 u_0},\qquad k=1,2,\ldots,N_c$$

$$\rho\frac{\partial Y_k}{\partial t}+\rho V\operatorname{grad}Y_k=\frac{1}{Re\,Sc}\operatorname{div}(\rho D_k\operatorname{grad}Y_k)-\varpi_k\frac{L}{\rho_0 u_0}$$
$$k=1,2,\ldots,N_c \tag{22}$$

where c_p and λ are the specific heat at constant pressure and thermal conductivity, respectively; T is the temperature; $c_{p,k}$ is the specific heat capacity at constant pressure for the kth component; $Y_k=\rho_k/\rho$ is the mass fraction of the kth component; ρ_k is the density of the kth component; D_k is the effective diffusion coefficient of the kth component; and h_k and ϖ_k are the enthalpy and reaction rate of the kth species. (Here reaction rate means value of mass consumed or produced per unit volume per unit time, e.g., gram per cubic centimeter per second.)

The variables (x, r, t), (u, v), and $(\rho, p, T, c_p, \mu, \lambda)$ in the system of Eqs. (17–22) are nondimensional. To nondimensionalize the variables, the following parameters were used: ρ_0, μ_0, L_0, and u_0, where the zero index is used from here on to denote the parameters at known fixed conditions. Then, too,

$$(x,r)=(\tilde{x},\tilde{r})/L_0,\qquad t=\tilde{t}u_0/L_0,\qquad (u,v)=(\tilde{u},\tilde{v})/u_0$$
$$\rho=\tilde{\rho}/\rho_0,\qquad T=\tilde{T}/T_0,\qquad \mu=\tilde{\mu}/\mu_0$$
$$\lambda=\tilde{\lambda}/\lambda_0,\qquad D=\tilde{D}/D_0,\qquad c_p=\tilde{c}_p/c_{p,0}$$

$Re=\rho_0u_0L_0/\mu_0$ is the Reynolds number, $Pr=\mu_0c_{p,0}/\lambda_0$ is the Prandtl number, $Sc=\mu_0/\rho_0D_0$ is the Schmidt number, and $Fr^2=u_0^2/aL_0$ is the Froude number square. The following normalization parameters were used: $u_0=1$ cm/s, $L_0=0.001$ cm, $\rho_0=1.177\times10^{-3}$ g/cm^3, $\lambda_0=1.983\times10^{-4}$ W/(cm·K), $c_{p,0}=\lambda_0/\mu_0$, and $D_0=\mu_0/\rho_0$.

Because the process develops at almost constant pressure, it appears sufficient to take into account only the temperature dependencies of thermophysic and transport functions that are included in the mathematical model of the process [Eqs. (17–22)].

The choice of small-scale heated domains (typical scale of the heat release region is ~10–100 μm) provides the possibility to limit ourselves to taking into account only molecular viscosity and heat conductivity, which, however, due to strong dependence on the temperature, are spatial coordinate functions, which must be taken into account in the calculations.

IV. Chemical Kinetics Models

Two kinetic models of global chemical reactions are used in this study. A common formulation for both models is

$$\sum_{m}^{N_c}a_{l,m}[Y]_m^{(r)}\xrightarrow{k_1}\sum_{m}^{N_c}b_{l,m}[Y]_m^{(p)},\qquad l=1,2,\ldots,N_r \tag{23}$$

where $a_{l,m}$ and $b_{l,m}$ are the stoichiometric coefficients for the lth global chemical reaction, m is the conventional number of reagents r and products p for the lth reaction, $[Y]_m^{(r)}$ and $[Y]_m^{(p)}$ are the molar concentrations of reagents and products, and N_c is the number of the effective chemical components taking into account in the N_r chemical reactions.

The first utilized model for the chemical kinetics for heterogeneous propellant burning was that suggested in Ref. 5. This model consists of three global reactions for eight chemical component. These are

$$a_{1,1}[Y_1]+a_{1,2}[Y_2]\rightarrow b_{1,1}[Y_3]+b_{1,2}[Y_4] \tag{24a}$$

$$a_{2,1}[Y_5]+a_{2,2}[Y_2]\rightarrow b_{2,1}[Y_6]+b_{2,2}[Y_7] \tag{24b}$$

$$a_{3,1}[Y_3]+a_{3,2}[Y_6]\rightarrow b_{3,1}[Y_8] \tag{24c}$$

where $[Y_k]$ are the molar concentrations of the global reactions effective components. Correspondence between conventional numbers of the effective chemical components and name of the real chemical components is presented in Table 1. Effective chemical components named P_1, P_2, and P_3 are the products of the global chemical reactions, containing all equilibrium products of the heterogeneous propellants [on the base of ammonium perchlorate (AP) and hydroxyl-terminated polybutadiene binder (HTPB) burning].

Taking into account the relation between the names and numbers of the effective chemical components, the rates for the global reactions may be written in the following form:

$$\dot{\omega}_1=k_1(T)(\rho_1/W_1)(\rho_2/W_2) \tag{25a}$$

$$\dot{\omega}_2=k_2(T)(\rho_5/W_5)(\rho_2/W_2) \tag{25b}$$

$$\dot{\omega}_3=k_3(T)(\rho_3/W_3)(\rho_6/W_6) \tag{25c}$$

where W_k is the molecular weight of the species k. Here the dimension for the $\dot{\omega}_k$ is mole per cubic centimeter per second.

The global chemical reactions constants are expressed by the Arrhenius law as

$$k_l(T)=A_l\exp(-E_l/R_0T) \tag{26}$$

where E_l is the activation energy, A_l is the preexponent factor (Table 2), and R_0 is the universal gas constant $R_0=1.9858$ cal/(mol·K). The stoichiometric coefficients of the kinetic mechanism (24) take into account actual correlations between chemical components. For the detailed kinetic mechanism see Ref. 5.

Table 1 Chemical components taken into account in the eighth component kinetic model

Conventional name of effective chemical component	Name of effective chemical component	$(Y_{k,w})_{AP}$	$(Y_{k,w})_{HTPB}$
Y_1	NH_3	0.054	0
Y_2	$HClO_4$	0.0214	0
Y_3	O_2	0.219	0
Y_4	P_1	0.7056	0
Y_5	C_4H_6	0	0.094
Y_6	CO	0	0.03
Y_7	P_2	0	0.104
Y_8	P_3	0	0.772

Table 2 Constants for the global chemical reactions rates in the eighth component model[a]

Number of reaction l	A_l, cm^3 s/mole	E_l, cal/mol
1	1.8×10^{14}	15,236
2	4.0×10^{14}	14,955
3	5.3×10^{13}	24,200

[a]Stoichiometric coefficients: $a_{1,1}=1$, $a_{1,2}=0.526$, $b_{1,1}=0.787$, $b_{1,2}=1.68$, $a_{2,1}=1$, $a_{2,2}=0.360$, $b_{2,1}=1.750$, $b_{2,2}=1.66$, $a_{3,1}=1.92$, $a_{3,2}=1.000$, $b_{3,1}=3.05$, and $b_{3,2}=0$.

Table 3 Chemical components taken into account in the fifth component kinetic model

Conventional name of effective chemical component	Name of effective chemical component	$(Y_{k,w})_{AP}$	$(Y_{k,w})_{HTPB}$
$Y_1 \equiv F_A$	NH_3	0.05	0
$Y_2 \equiv Ox$	$HClO_4$	0.07	0
$Y_3 \equiv P_1$	P_1	0.88	0
$Y_4 \equiv F_B$	C_4H_6	0	1
$Y_5 \equiv P_2$	P_2	0	0.9

Table 4 Constants for the global chemical reactions rates in the fifth component model[a]

Number of reaction l	A_l, cm^3 s/mole	E_l, cal/mol
1	2.52×10^{13}	15,236
2	2.52×10^{14}	14,955

[a]Stoichiometric coefficients: $a_{1,1} = 1, a_{1,2} = 0.526$, $b_{1,1} = 2.68, a_{2,1} = 1, a_{2,2} = 0.36$, and $b_{2,1} = 2.67$.

The species reaction rates for Eqs. (21) and (22) are calculated by using the obvious relations, for example, $\varpi_1 = -a_{1,1} W_1 \dot{\omega}_1$, $\varpi_2 = -(a_{1,2}\dot{\omega}_1 + a_{2,2}\dot{\omega}_2) W_2$, etc., where the dimensions of all reaction rates are gram per cubic centimeter per second.

The second simplified model of the chemical kinetics for heterogeneous propellant burning was developed in Ref. 4. The model consists of two global reactions for five chemical components, presented in Table 3. These are

$$a_{1,1}[Y_1] + a_{1,2}[Y_2] \rightarrow b_{1,1}[Y_3] \tag{27a}$$

$$a_{2,1}[Y_4] + a_{2,2}[Y_2] \rightarrow b_{2,1}[Y_5] \tag{27b}$$

where $Y_2 = Ox$, $Y_1 = F_A$, and $Y_4 = F_B$ are the reagents (oxidizer Ox and fuel F_A correspond to the AP and F_B corresponds to the binder); $Y_3 = P_1$ and $Y_5 = P_2$ are the products of the global chemical reactions, containing all equilibrium products of the heterogeneous propellants (on the base of AP and HTPB) burning.

The rates for the global reactions are then (see also Table 4)

$$\dot{\omega}_1 = k_1(T)(\rho_1/W_1)(\rho_2/W_2) \tag{28a}$$

$$\dot{\omega}_2 = k_2(T)(\rho_4/W_4)(\rho_2/W_2) \tag{28b}$$

V. Thermodynamic and Transport Properties of the Gas Phase

For determining the thermophysical and transport properties of the gas mixture the following relations were used:

$$p = \rho \frac{R_0}{W_\Sigma} T, \qquad \rho = \sum_k^{N_c} \rho_k$$

$$c_p = \sum_k^{N_c} c_{p,k} Y_k, \qquad W_\Sigma = \frac{1}{\sum_k^{N_c} (Y_k/W_k)} \tag{29}$$

To approximate the thermodynamic properties the following approximations are used for the specific heat and the enthalpy[6]:

$$c_{p,k} = A + Bt + Ct^2 + Dt^3 + E/t^2, \qquad \text{J/(mol·K)}$$

$$h_k - h_{k,T=298.15K} = At + Bt^2/2 + Ct^3/3 + Dt^4/4 - E/t + F - \Delta H^0_{f,298}, \qquad \text{kJ/mol} \tag{30}$$

where $t = T/1000$, $\Delta H^0_{f,298.15}$ is the enthalpy of formation at 298.15 K, and A, B, C, D, E, and F are the approximation coefficients given in Ref. 6.

Table 5 Approximation coefficients for products enthalpy of the global chemical reactions for the eighth component model

Number of reaction	A_{P_k}, cal/mole	B_{P_k}, cal/(mol·K)
1	−60,054	10.3
2	−40,000	12.2
3	−78,857	12.6

Table 6 Approximation coefficients for products enthalpy of the global chemical reactions for the fifth component model

Number of reaction	A_{P_k}, cal/mole	B_{P_k}, cal/(mol·K)
1	−59,000	10
2	−37,000	12

The average molecular weights of products of the eighth component global chemical reactions and approximations for enthalpy are taken from Ref. 5 (Table 5). Thus,

$$W_{P_1} = 28.41, \qquad W_{P_2} = 24.69, \qquad W_{P_3} = 29.3, \qquad \text{g/mol}$$

$$h_{P_k} = A_{P_k} + B_{P_k} T, \qquad k = 1, 2, 3 \tag{31}$$

For the fifth component global chemical reactions, the following values were used (see also Table 6):

$$W_{P_1} = W_{P_2} = 29, \qquad \text{g/mol}$$

$$h_{P_k} = A_{P_k} + B_{P_k} T, \qquad k = 1, 2 \tag{32}$$

Average characteristics for the momentum, heat, and mass transfer coefficients assumed that

$$\mu(T) = 1.983 \times 10^{-4} \frac{273 + 117}{T + 117} \sqrt{\left(\frac{T}{273}\right)^3} \quad \text{g/(cm·s)} \tag{33}$$

$$\lambda(T) = \frac{\mu c_p}{Pr_*}, \qquad D_k = D(T) = \frac{\mu}{\rho Sc_*} \tag{34}$$

Setting $Pr_* = 1$ and $Sc_* = 1$, the following relations will be used: $\lambda(T) = \mu c_p$ and

$$D_k = D(T) = \mu/\rho \tag{35}$$

VI. Boundary Conditions

First we will formulate the boundary conditions for solving Eqs. (17–22) in relation to the velocity, temperature, and mass fractions of the chemical components.

Boundary Conditions at $x = 0$ (Surface of the Heterogeneous Material)

Mass Fractions Distributions Along the Surface

At $y < y_1$ (AP surface) for the eighth component model (see Table 1)

$$Y_k = Y_{k,w}, \qquad k = 1, 2, 3, 4, \qquad Y_k = 0, \qquad k = 5, 6, 7, 8 \tag{36a}$$

For the fifth component model (see Table 3)

$$Y_k = Y_{k,w}, \qquad k = 1, 2, 3, \qquad Y_k = 0, \qquad k = 4, 5 \tag{36b}$$

At $y_1 < y < L$ (binder surface) for the eighth component model (see Table 1)

$$Y_k = 0, \qquad k = 1, 2, 3, 4, \qquad Y_k = Y_{k,w}, \qquad k = 5, 6, 7, 8 \tag{37a}$$

For the fifth component model (see Table 3)

$$Y_k = 0, \qquad k = 1, 2, 3, \qquad Y_k = Y_{k,w}, \qquad k = 4, 5 \tag{37b}$$

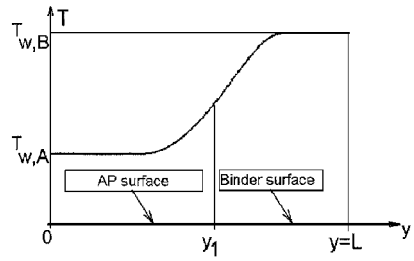

Fig. 2 Postulated temperature distribution on the AP/HTPB surface.

Temperature T_w and Injection Velocity u_w Distributions Along the Surface

We depict a continuous variation for the surface temperature bounding the oxidizer/fuel by assuming

$$T_w = T_m - (2/\pi)\Delta_T \arctan[(y - y_1)/\beta_y] \tag{38a}$$

$$u_w = u_m - (2/\pi)\Delta_u \arctan[(y - y_1)/\beta_y] \tag{38b}$$

where

$$T_m = 0.5(T_{w,A} + T_{w,B}), \qquad u_m = 0.5(u_{w,A} + u_{w,B})$$

$$\Delta_T = 0.5(T_{w,A} - T_{w,B}), \qquad \Delta_u = 0.5(u_{w,A} - u_{w,B})$$

$$T_{w,A} = \frac{1}{y_1}\int_0^{y_1} T_w\,\mathrm{d}r, \qquad T_{w,B} = \frac{1}{L - y_1}\int_{y_1}^{L} T_w\,\mathrm{d}r$$

$$u_{w,A} = \frac{1}{y_1}\int_0^{y_1} u_w\,\mathrm{d}r, \qquad u_{w,B} = \frac{1}{L - y_1}\int_{y_1}^{L} u_w\,\mathrm{d}r$$

The last four integrals could be considered as the mean values for the surface temperature and blowing velocity. The parameter β_y specifies conditions of heat transfer between layers of oxidizer and binder in solid phase. A typical distribution of surface temperature is shown in Fig. 2.

Boundary Conditions at the Symmetry Plane ($y = 0$)

Where $y = 0$ and $v = 0$,

$$\frac{\partial u}{\partial r} = \frac{\partial T}{\partial r} = \frac{\partial Y_k}{\partial r} = 0, \qquad k = 1, 2, \ldots, N_c \tag{39}$$

Boundary Conditions at the Symmetry Plane ($y = L$)

Where $y = L$ and $v = 0$,

$$\frac{\partial u}{\partial r} = \frac{\partial T}{\partial r} = \frac{\partial Y_k}{\partial r} = 0, \qquad k = 1, 2, \ldots, N_c \tag{40}$$

Boundary Conditions at the Upper Boundary of the Calculated Domain ($x \to \infty$)

Where $x \to \infty$,

$$\frac{\partial u}{\partial x} = \frac{\partial^2 v}{\partial x^2} = \frac{\partial T}{\partial x} = \frac{\partial Y_k}{\partial x} = 0, \qquad k = 1, 2, \ldots, N_c \tag{41}$$

The downstream dimensions for the computational domain to approximate the infinity conditions are varied and range from 200 to 500 μm (typical size of burning area is about 5–20 μm). The dimensions of the computational domain ($x = H$) at which the impact of uncertainty in the boundary conditions for the velocity components was negligible were identified by numerical experiments.

The boundary conditions for identification of the dynamic variables ω, Ψ, and ε are as follows:

$$y = 0, \qquad \omega = 0, \qquad \Psi = 0, \qquad \frac{\partial \varepsilon}{\partial y} = 0$$

$$x = 0, \qquad \omega = -\left.\frac{\partial \rho u}{\partial y}\right|_w, \qquad \Psi = \int_0^y \rho_w u_w\,\mathrm{d}y, \qquad \varepsilon = 0$$

$$y = L: \qquad \omega = 0, \qquad \Psi = \int_0^L \rho_w u_w\,\mathrm{d}y, \qquad \frac{\partial \varepsilon}{\partial y} = 0$$

$$x \to \infty (x = H): \qquad \frac{\partial \omega}{\partial x} = 0$$

$$\Psi = \int_0^y \exp[\varepsilon(x = H)]\rho(x = H)u(x = H)\,\mathrm{d}y, \qquad \frac{\partial \varepsilon}{\partial x} = 0$$

VII. Initial Conditions

To obtain steady-state solutions, the following initial conditions were used:

$$t = 0: \qquad v(x, y) = 0, \qquad u(x, y) = u_w, \qquad T(x, y) = T_w$$

$$Y_k(x, y) = Y_{k,w}, \qquad k = 1, 2, \ldots, N_c \tag{42}$$

The pressure is assumed to be constant and equal to p_0. Also to obtain a unsteady solution to the problem, steady-state solutions were used to provide initial nodal conditions throughout the domains.

VIII. Sequence of General Problem Solution and Method of Numerical Integration

An iterative solution process at each time step consisted of three consecutive stages, which can be conventionally called energy, gasdynamic, and species transport stages. At the energy stage Eq. (21) was solved, and the velocity fields were assumed to be fixed. Because of the strong nonlinear dependence of temperature on the burning processes, it is necessary to arrange an additional iterative process to the solution of Eqs. (21) and (22) but only after solution of the gasdynamic equations.

After an energy conservation equation is initially solved, the density field is defined, and the gasdynamic stage of the problem solution starts. The sequence of solution of the equations is as follows: Eqs. (19), (17), (18), and (20). The density field in this case is fixed in space. Convergence of the iterative process is monitored with functions ω, ρu, and ρv.

The species transport stage starts after the gasdynamic stage, and then iterations for a given time step are repeated from the energy conservation equation. The number of internal iterations within the energy, gasdynamic, and species transport stages is determined first by the selected time integration step $\tau = t^{p+1} - t^p$. The optimal step is the one that does not require additional iterations between the internal stages. Numerical calculations established that, for this case, the total computational time was the shortest.

All finite-difference equations were presented in a canonical form of a five-point difference equation, as follows:

$$A_{i,j}U_{i-1,j} + B_{i,j}U_{i+1,j} + \bar{A}_{i,j}U_{i,j-1} + \bar{B}_{i,j}U_{i,j+1} - C_{i,j}U_{i,j} + F_{i,j} = 0$$

where $U = \{\omega, \Psi, \varepsilon, T, Y_k\}$, and $A_{i,j}$, $B_{i,j}$, $\bar{A}_{i,j}$, $\bar{B}_{i,j}$, $C_{i,j}$, and $F_{i,j}$ are the approximation coefficients of the finite difference scheme.

The finite difference scheme has hybrid first–second order of accuracy in space. The donor cells scheme[1] or second-order central-differences schemes were used for an approximation of the transfer members in all equations. (In the considered cases we did not use any computational flux corrected methods.) All finite difference equations were solved by the successive overrelaxation in lines method.[7]

IX. Calculated Results

Two problems concerning gasdynamic structure of microflames above the surface of burning heterogeneous rocket propellants on the base of AP (oxidizer) and HTPB (fuel, binder) were solved.

In the first problem, the process of the gasdynamic structure reorganization due to periodical replacement of the oxidizer and the binder surfaces was considered.

In the second problem, the structure of a microflame above a burning surface was studied for rapid modification of mass forces stipulated by a modification of gravitational acceleration.

Note that detailed reviews of a state of the art of computing investigations of solid propellants burning processes were recently summarized and published in Refs. 8–10. Also, the statements of the problems of solid propellants heterogeneous burning in the present

paper is similar in many aspects to those considered in Ref. 4. Nevertheless, the processes calculated here were not discussed in the referenced works. In addition, note that gasdynamic problems of heterogeneous solid propellants burning are considered here only as an illustration of UDV method application; therefore, some additional simplified assumptions concerning proper burning processes are used here.

A. Analysis of Changes of Gasdynamic Structure of Microflame at Alternation of Oxidizer and Binder Surfaces

A schematic of the problem is shown in Fig. 1 and is based on the following assumptions:

1) The mass burning velocities of the oxidizer and binder are not equal and do not change with time, at least in the period of the oxidizer and binder alternation, but because they have different densities, the composite material surface remains flat during the burnout process. (Note that this assumption is generally not correct. However, in accord with Ref. 11 there are some conditions for the oxidizer/binder layered system burning when this assumption is approximately true.)

2) After burnout of the composite material layer by a thickness δ (this magnitude is determined by a characteristic size of the oxidizer grains), the oxidizer surface is instantly replaced by the binder surface, and conversely the binder surface is instantly replaced by the oxidizer surface; at least this time is much less than the period of the oxidizer and binder alternation.

3) Processes of a quenching and ignition of the composite material components are considered as very fast (compared to the investigated timescales); gasdynamic processes accompanying the quenching/ignition processes are modeled to be very fast and are not taken into account.

The purpose of the study is to determine the characteristic temporal scales, on which the microflame gas structures are stabilized due their locations above the oxidizer and the fuel binder.

The numerical simulation results have shown that dynamics of a microflame depends on many factors, such as pressure in gas, volumetric ratio of an oxidizer and binder φ, surface temperatures, and the velocities of the injected gases from burning surfaces. Therefore, the few calculated results only illustrate some common characteristics of the processes but do not describe all possible variants.

To estimate a time of a microflame gasdynamic structure installation, one can use a period of thermogravitation convection (for small injection velocities) or characteristic time of forced convection (for large injection velocities).

A characteristic velocity of thermogravitation movement is $u_{\text{grav}} = \sqrt{(gL^*)} = 2.2$ cm/s, for $L^* = 0.005$ cm, and the characteristic injection velocity of combustion products from the burning surface is $u_w = 5$–50 cm/s. With these values, the periods of thermogravitation and forced convection are nearly equal; accordingly, $\tau_{\text{grav}} = L^*/u_{\text{grav}} = 2.3$ ms and $\tau_{\text{conv}} = L^*/u_w = 1$–$0.1$ ms.

Assuming a linear burning velocity of a composite material as $\dot{r}_B = 1$ cm/s, then for typical size of the oxidizer granules $\delta = 0.005$ cm, the surfaces alternation period is equal to $\tau_{\text{alt}} = \delta/\dot{r}_B = 5$ ms. This means that the time for the microflame gasdynamic structure stabilization coincides with the period of surfaces alternations.

Note that in the estimates just discussed there is no pressure effect from the gas phase. Nevertheless, this parameter appears implicitly because the pressure determines a mass velocity of a composite material thermodestruction and also the injection velocity of gaseous burning products.

Our calculations have confirmed the correctness of these estimates. For these calculations the following basic data were set: $H = 0.03$ cm, $L = 0.01$ cm, $u_{w,A} = 49$ cm/s, $u_{w,B} = 13$ cm/s, $T_{w,A} = 866$ K, $T_{w,B} = 1140$ K, and $p_0 = 40$ atm. The period of the burning surfaces alternation was set to equal $\tau_{\text{alt}} = 5$ ms.

The five-component kinetic model is used in these calculations. Mass fractions of the effective components on the burning surface are given in the Table 3. The global chemical reaction rates constants and the stoichiometric factors are given in the Table 4.

Figure 3 shows steady-state temperature and velocity fields at the initial structure of the oxidizer, $0 < y < 0.0075$ cm, and

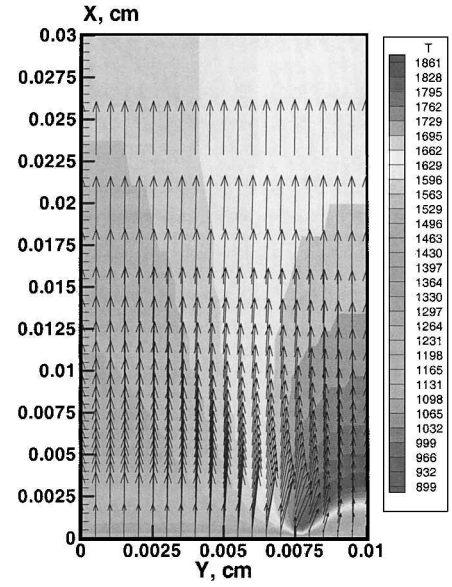

Fig. 3 Temperature and flowfield for the initial structure of AP ($y < 0.0075$ cm) and HTPB ($y > 0.0075$ cm); velocity magnitudes are $u_{w,A}$ ($y < 0.0075$ cm) = 49 cm/s and $u_{w,B}$ ($y > 0.0075$ cm) = 13 cm/s.

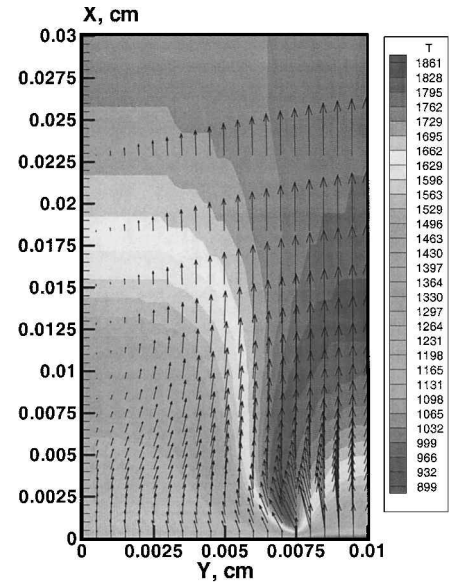

Fig. 4 Temperature and flowfield for the reverse structure of AP ($y > 0.0075$ cm) and HTPB ($y < 0.0075$ cm); velocity magnitudes are $u_{w,A}$ ($y > 0.0075$ cm) = 49 cm/s and $u_{w,B}$ ($y < 0.0075$ cm) = 13 cm/s.

the binder, $0.0075 < y < 0.01$ cm. The steady-state fields of the temperature and velocity for the alternate structure of the oxidizer ($0.0075 < y < 0.01$ cm) and the binder ($0 < y < 0.0075$ cm) are shown in Fig. 4. The transient of steady-state thermodynamic condition installation τ_{conv} has taken in this case approximately $0.3\tau_{\text{alt}}$.

One significant feature that is evident is the origin of the vortex gas motion in regions above the fuel binder $y < 0.0025$ cm and the oxidizer $0.0075 < x < 0.025$ cm.

B. Microflame Structure at Different Gravitational Accelerations

Changes of a thermodynamic structure of microflames due to modifications of gravitational acceleration were studied. The schematic is the same as that shown in Fig. 1. The eight-component kinetic model of three global chemical reactions was used. Mass fractions of the effective components in immediate proximity above the burning surface, global chemical reactions rates constants, and the stoichiometric coefficients are given in Tables 1 and 2.

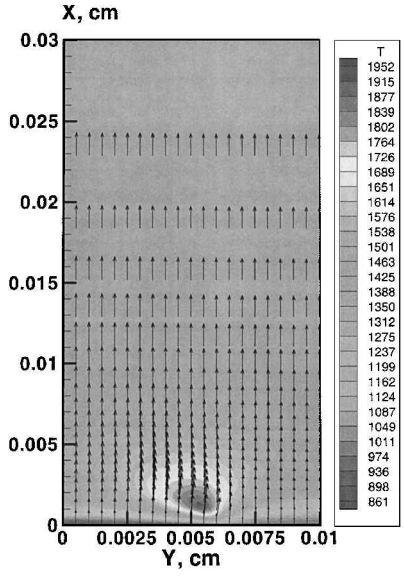

Fig. 5 Temperature and flowfield for $a = -g$ and $p_0 = 20$ atm; AP and HTPB are structured at $y < 0.006$ cm and $y > 0.006$ cm, correspondingly; velocity magnitudes are $u_{w,A}(y < 0.006\text{ cm}) = 10$ cm/s and $u_{w,B}(y > 0.006\text{ cm}) = 5$ cm/s.

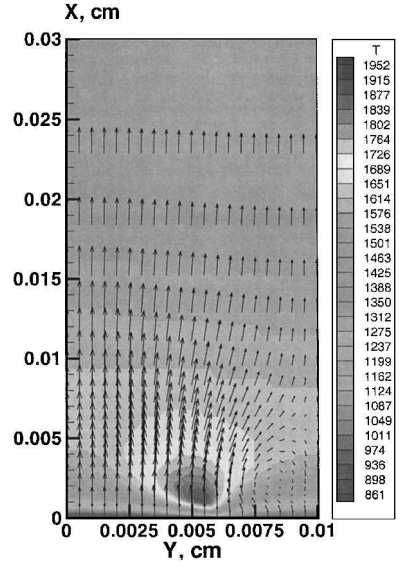

Fig. 6 Temperature and flowfield for $a = -10g$ and $p_0 = 20$ atm; AP and HTPB structured at $y < 0.006$ cm and $y > 0.006$ cm correspondingly; velocity magnitudes are $u_{w,A}(y < 0.006\text{ cm}) = 10$ cm/s and $u_{w,B}(y > 0.006\text{ cm}) = 5$ cm/s.

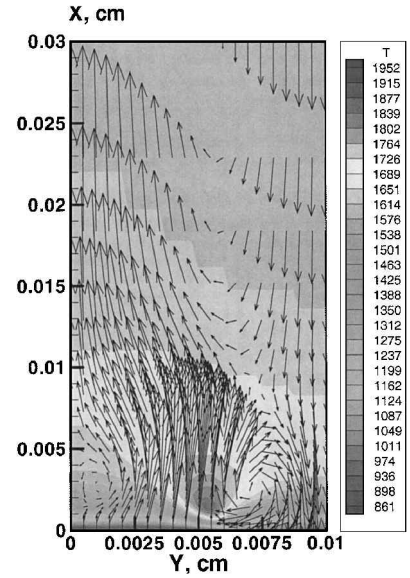

Fig. 7 Temperature and flowfield for $a = -100g$ and $p_0 = 20$ atm; AP and HTPB are structured at $y < 0.006$ cm and $y > 0.006$ cm correspondingly; velocity magnitudes are $u_{w,A}(y < 0.006\text{ cm}) = 10$ cm/s and $u_{w,B}(y > 0.006\text{ cm}) = 5$ cm/s.

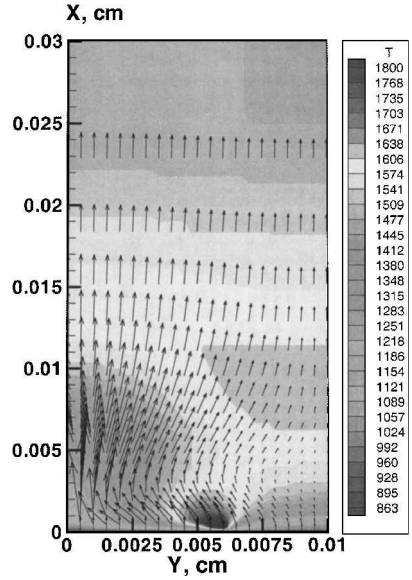

Fig. 8 Temperature and flowfield for $a = -g$ and $p_0 = 80$ atm; AP and HTPB are structured at $y < 0.006$ cm and $y > 0.006$ cm correspondingly; velocity magnitudes are $u_{w,A}(y < 0.006\text{ cm}) = 10$ cm/s and $u_{w,B}(y > 0.006\text{ cm}) = 5$ cm/s.

The calculations were conducted for the near surface area of the following sizes: $H = 0.03$ cm and $L = 0.01$ cm. The oxidizer takes 60% of the surface ($0 < y < 0.006$ cm) and the binder takes 40% ($0.006 < y < 0.01$ cm). Injection gas velocities from the surfaces and their temperatures were set as follows: $u_{w,A} = 10$ cm/s, $u_{w,B} = 5$ cm/s, $T_{w,A} = 823$ K, and $T_{w,B} = 950$ K.

In the first calculated series (when the pressure was set $p_0 = 20$ atm) the gravitational acceleration $a = -g = -981$ cm/s^2 was set at $a = -1, -10$, or $-100\,g$. The calculated microflame thermodynamic structure is shown in Figs. 5–7. It is clear that the gasdynamic structure of the microflame is noticeably altered by gravitational acceleration. For example, one can see approximately parallel gas motion in the whole computational domain at $a = -g$ (Fig. 5) and large-scale vortex gas motion above the binder surface at $a = -10\,g$ (Fig. 6), which is stipulated by the Archimedean forces. Just as the formation of a vortex motion above the binder surface, the formation of a vortex motion above the oxidizer surface is predicted at $a = -100\,g$ (Fig. 7). It is remarkable that the temperature fields for the three calculated series differ only slightly (compare Figs. 5–7). Note that the thermodynamic structure of microflames shown in Figs. 5–7 corresponds to a steady-state solution.

The pressure in gas phase was increased up to $p_0 = 80$ atm in the second calculated series. Calculated results for the conditions at $a = -g$ and $-10\,g$ are shown in Figs. 8 and 9, respectively. One can see that changes in temperature fields are insignificant as the gravitational acceleration increases. However, the gasdynamic structure is changed rather noticeably. A large-scale vortex motion is predicted to appear directly above the burning surface when $a = -10\,g$ (Fig. 9b) due to the differences in the gas velocities injected above the solid binder and oxidizer at this large pressure, $p = 80$ atm.

Note the temperature gradients increase near the surface with growth of the gas pressure (compare Figs. 5 and 8), which confirms the well-known fact of increasing heat fluxes to a surface for increasing pressure.

Figure 10 shows the calculated results for the opposite direction of a gravity acceleration ($a = +10\,g$) at pressure $p_0 = 20$ atm.

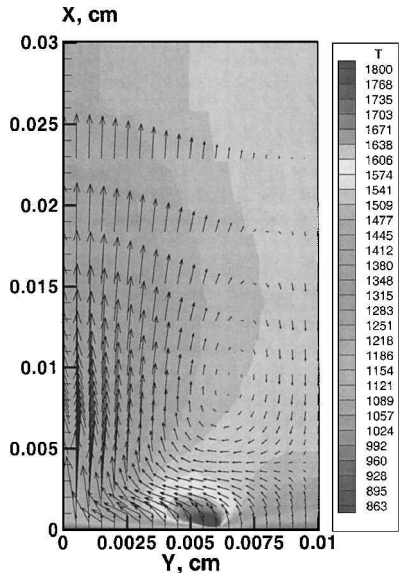

Fig. 9 Temperature and flowfield for $a = -10\,g$ and $p_0 = 80$ atm; AP and HTPB are structured at $y < 0.006$ cm and $y > 0.006$ cm correspondingly; velocity magnitudes are $u_{w,A}(y < 0.006\text{ cm}) = 10$ cm/s and $u_{w,B}(y > 0.006\text{ cm}) = 5$ cm/s.

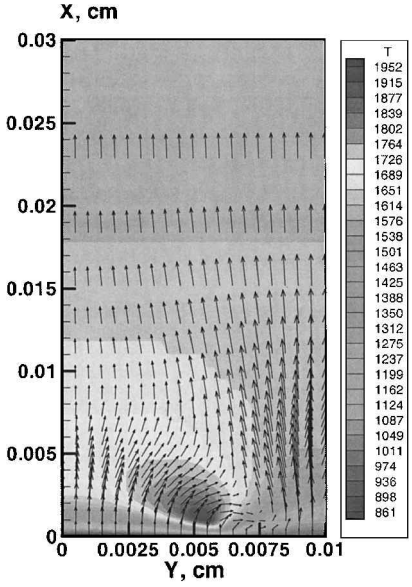

Fig. 10 Temperature and flowfield for $a = +10\,g$ and $p_0 = 20$ atm; AP and HTPB are structured at $y < 0.006$ cm and $y > 0.006$ cm correspondingly; velocity magnitudes are $u_{w,A}(y < 0.006\text{ cm}) = 10$ cm/s and $u_{w,B}(y > 0.006\text{ cm}) = 5$ cm/s.

When Figs. 6 ($a = -10\,g$) and 10 ($a = +10\,g$) are compared, one can conclude that a minor modification in a temperature fields and noticeable modification of gasdynamic structure of the microflames are predicted. In the case of positive gravity acceleration, the suppression of a vortex structure of gas flows above the surface is observed.

X. Conclusions

The paper introduced the UDV method intended for integration of the Navier–Stokes equations in conditions of subsonic movements of gases for any local density changes. This magnitude of the density differences is stipulated by local heat of gas due to chemical reactions or any other volumetric source of heat.

The general idea of the UDV method consists in the introduction of a new function, defined as local density change in time, which allows use of the well-known method of dynamic variables (vortex–stream function) for numerical integration of the Navier–Stokes equations, even for cases of unsteady compressible flows. This method was used for the numerical investigation of two problems concerned with the thermodynamic structure of microflames near a surface of burning composite rocket propellant on the base of AP/HTPB.

The influence of alternate AP/binder layers at the burning surfaces of oxidizer and binder on changes in a microflame structure was investigated in the first series of calculations. It was shown that it is necessary to take into account not only space heterogeneity of the composite materials, but also the unsteady character of the gasdynamic processes near the surface.

The influence of magnitude and direction of gravitational acceleration on the structure of a microflame is investigated in the second series. It was shown that the variation of the gravitational acceleration to two orders has a minor effect on the temperature fields near the burning surface, but significantly influences the gasdynamic structure of microflames. When the magnitude and direction of a gravitational acceleration was depended on, the appearance or, on the contrary, suppression of a large-scale rotational structure was predicted.

Acknowledgments

The Center for Simulations of Advanced Rockets (CSAR) research program is supported by the U.S. Department of Energy through the University of California under Subcontract B341494. We acknowledge Robert Fiedler, CSAR staff scientist, for helpful discussions and assistance in the numerical calculations. Also important discussions with Robert Glick were very useful in studying the effects on the burning processes due to enhanced gravitational acceleration.

References

[1] Roache, P. J., *Computational Fluid Dynamics*, Hermosa, Albuquerque, NM, 1976.

[2] Oran, E. S., and Boris, J. P., *Numerical Simulation of Reactive Flows*, Elsevier, New York, 1988.

[3] Fang, K. C., Osswald, G. A., Ghia, K. N., and Ghia, U., "Numerical Simulation of Low-Speed Unsteady Wake Development Behind Airfoils, Using Incompressible and Compressible Analyses," AIAA Paper 2001-0298, Jan. 2001.

[4] Surzhikov, S. T., Murphy, J. J., and Krier, H., "2D Model for Unsteady Burning of Heterogeneous AP/Binder Solid Propellants," AIAA Paper 2000-3573, July 2000.

[5] Ermolin, N. E., Korobeinichev, O. P., Fomin, V. M., and Chernov, A. A., "Study of Flame Structure for Mixed Solid Fuels Based on Ammonium Perchlorate and Polybutadiene Rubber," *Combustion, Explosion, and Shock Waves*, Vol. 28, No. 4, 1992, pp. 59–65.

[6] *Chemistry Web Book*, URL: http://webbook.nist.gov [2000].

[7] Tannehil, J. C., Anderson, D. A., and Pletcher, R. H., *Computational Fluid Mechanics and Heat Transfer*, Taylor and Francis, Washington, DC, 1997.

[8] Yang, V., Brill, T. B., and Ren, W.-Z. (eds.), *Solid Propellant Chemistry, Combustion, and Motor Interior Ballistics*, Vol. 185, Progress in Astronautics and Aeronautics, AIAA, Reston, VA, 2000.

[9] Jackson, T. L., and Buckmaster, J., "Nonpremixed Periodic Flames Supported by Heterogeneous Propellants," *Journal of Propulsion and Power*, Vol. 16, No. 3, 2000, pp. 498–504.

[10] Knott, G. M., and Brewster, M. Q., "Two-Dimensional Combustion Modeling of Heterogeneous Solid Propellants with Finite Peclet Number," *Combustion and Flame*, Vol. 121, 2000, pp. 91–106.

[11] Price, E. W., Sambamurthi, J. K., Sigman, R. K., and Panyam, R. R., "Combustion of Ammonium Perchlorate-Polymer Sandwiches," *Combustion and Flame*, Vol. 63, 1986, pp. 381–413.

K. Kailasanath
Associate Editor